Electrochemiluminescent immunoassay enhancement driven by carbon nanotubes

Electrochemiluminescent immunoassay enhancement driven by carbon nanotubes

Sara Rebeccani,[a] Cecilia Wetzl,[b] Valeria Anna Zamolo,[c] Alejandro Criado,*[b,d] Giovanni Valenti,*[a] Francesco Paolucci,[a] and Maurizio Prato[b,c,e]

Electrochemiluminescence (ECL) is a leading analytical technique for clinical monitoring and early disease diagnosis. Carbon nanotubes are used as efficient nanomaterials for ECL signal enhancement providing new insights into the mechanism for the ECL generation but also affording application in beads-based immunoassay and ECL microscopy-based bioimaging.

Biomarkers are biological indicators with a key role in identifying human body function changes. Recently, the quantitative detection of biomarkers is even more important in clinical monitoring implementation and early screening of cancer and other diseases. More sensitive and specific sensors are developed for the detection of low concentrations of biomarkers in complex matrices like blood and other biofluids.[1,2] The quantification of biomarkers is essential in the management of the actual pandemic scenario and the prevention of future epidemics.[3]

In this context, electrochemiluminescence (ECL) is a leading technique in the field of immunoassays-based biomarker detection and biosensors fabrication.[4–8] The widespread and growth of ECL are due to its advantageous features as the satisfactory signal-to-noise ratio,[9,10] good spatial and temporal control and signal generation in an aqueous environment that allows the analysis in real and complex matrices.[11] In commercial ECL-based immunoassays, such as Elecsys® immunoassays,[12] the biomarkers are detected after their immobilization on the working electrode through magnetic beads, attracted to the electrode surface using a magnet.[13]

In this study, the ECL beads-based assay is combined with carbon nanotubes to optimize the ECL active layer and activate a more efficient ECL mechanism. Carbon nanotubes are unique nanomaterials largely used in ECL especially for biosensors based on $[Ru(bpy)_3]^{2+}$ /TPrA.[14–17] However, the mechanism of ECL enhancement in beads-based assay remains underexplored. Here we exploit an ECL mechanism, activated by the presence of functionalized carbon nanotubes (f-CNT), for enhance the ECL signal.

ECL has been used, in combination with microscopy, as surface confined technique for the visualization of objects[18–23] and for mapping and quantifying analytes at electrode surface.[24,25] Although this technique shows great spatial resolution, it has to be optimized to further extend and control the thin layer from the electrode, in which the objects can be visualized, which is limited by the short lifetime of the electrogenerated coreactant radicals.[26–28] Therefore, different approaches have been applied for controlling the ECL active layer, underlining how promising is the technique for sensor application.[5,13,29–35]For example, the application of the so-called Faraday cage for extending the ECL emission layer, in which luminophores becomes a part of the electrode, is an innovative and efficient approach for the improvement of the technique.[36] In this context, nanotechnologies have a pivotal role in the implementation of the ECL signal.[37] The successful and promising combination between carbon-based nanomaterial and ECL were deeply studied, owing to the unique and advantageous features, such as fast kinetics for the amines oxidation.[30,38–42]

Herein, functionalized carbon nanotubes were applied for optimizing the distribution of the ECL-emitting layer (see Fig.1). This approach allows the increase of the ECL active layer and enhancement of the signal through a combination of two different ECL generation mechanisms. To mimic the real beads-based commercial immunoassays, the effect of f-CNT on micron-sized magnetic beads functionalized with a biotinylated carbon nanotube labeled with $[Ru(bpy)_3]^{2+}$ complex was

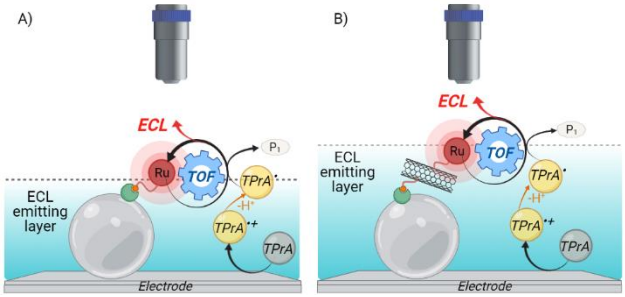

Figure 1. "Oxidative-reduction" coreactant mechanisms for the electrochemiluminescent emission of micromagnetic beads (light grey sphere) systems (biotin,red circle, and streptavidin, green shape), involving TPrA as coreactant and $[Ru(bpy)_3]^{2+}$ as luminophore. A) Only TPrA is oxidized on the electrode. B) $[Ru(bpy)_3]^{2+}$ is also oxidized on the double-walled carbon nanotubes (f-CNTs). Created with BioRender.com.

investigated. Carbon nanotubes can create a conductive layer around the beads, extending the ECL active layer and enhancing the ECL signal through the direct oxidation of the luminophore on this new conductive layer. This latter mechanism is not active in conventional bead system, in which the direct oxidation of the luminophores is neglected.[13,43,44]

The most important ECL application is based on the so-called "oxidative reduction" coreactant mechanism for ECL generation, in which TPrA is used as the sacrificial coreactant and tris(2,2'-bipyridyl) ruthenium (II), $[Ru(bpy)_3]^{2+}$, as the luminophore.[43,45–47] This

mechanism was largely investigated and the species involved are the protagonists in the field of ECL biosensors and imaging for emission detection of objects close to the electrode surface (within 3 μm from the electrode surface). The commercialized immunosystem involved micromagnetic beads functionalized with the biotinylated antibodies labeled with $[Ru(bpy)_3]^{2+}$ and TPrA as coreactant.[12,13] In this mechanism, also called *remote ECL*, TPrA is oxidized (Figure 1A) at the electrode to the corresponding radical cation $TPrA^{\bullet+}$, and $TPrA^{\bullet}$ radicals are produced after a deprotonation step (1–3). $TPrA^{\bullet}$ reduces the luminophore (4) that is subsequently oxidized to the excited state by $TPrA^{\bullet+}$ (5)[13,43]

$$TPrAH^+ \leftrightarrows TPrA + H^+ \quad (1)$$

$$TPrA - e^- \leftrightarrows TPrA^{\bullet+} \quad (2)$$

$$TPrA^{\bullet+} \leftrightarrows TPrA^{\bullet} + H^+ \quad (3)$$

$$TPrA^{\bullet} + \left[Ru(bpy)_3\right]^{2+} \leftrightarrows P1 + \left[Ru(bpy)_3\right]^{+} \quad (4)$$

$$TPrA^{\bullet+} + \left[Ru(bpy)_3\right]^{+} \leftrightarrows TPrA + \left[Ru(bpy)_3\right]^{2+*} \quad (5)$$

$$\left[Ru(bpy)_3\right]^{2+*} \rightarrow \left[Ru(bpy)_3\right]^{2+} + h\nu \quad (6)$$

where P1 is the product of the homogeneous TPrA• oxidation.

According to the mechanism outlined above, because of the limited $TPrA^{\bullet+}$ lifetime,[13,43] emission may only occur from luminophores located within few micrometers (~3 μm) from the electrode surface; this is among the major intrinsic limiting factors for the signal intensity.[48] Additionally, the ECL distribution around the beads is not homogeneous, depending on the decaying radicals distribution.[13] High intensity can, in principle, be obtained by increasing the distance from the electrode surface, in which both radicals are present in sizeable amounts, and also to involve an increased fraction of fluorophores in the ECL-generating process.

In this context, functionalized carbon nanotubes (CNT-Ru) were prepared with a double functionalization of oxidized DWCNTs, by combining 1,3 dipolar cycloaddition reaction and amidation of carboxylic groups to sequentially introduce: i) the $[Ru(bpy)_3]^{2+}$ complex as a luminophore, and ii) an amine functional group to link biotin as biorecognition element (Figures 2 and S1–2). Thus, the biotin moiety is used for the attachment of this material onto micromagnetic beads. The above approach provided tubes with a controllable labeling capability and high surface area, and whose electronic properties were still highly preserved. As such, they proved to promote the fast electrochemical oxidation of amines very efficiently, once deposited onto the electrode surface. Fluorescence spectra and mass analysis confirmed the functionalization of CNTs (Figure S3 and table S1), whose structure was analyzed by TEM imaging, TGA, and Raman spectroscopy (Figures S4–6).

CNT-Ru was used for micromagnetic beads functionalization through the biotin-streptavidin strong bonding (beads@CNT-Ru Figures S5–7). The functionalized beads were then immobilized by a magnet onto a platinum electrode and their ECL emission was integrated using an ECL-microscope in the presence of 180 mM of TPrA. The ECL emission from beads@CNT-Ru was then compared with that measured on standard 2.8 μm microbeads functionalized with a biotinylated antibody labeled with $[Ru(bpy)_3]^{2+}$ complex (beads@Ru).

An increase of ~4 times in the ECL intensity integrated over single beads@CNT-Ru (Figure 3A and Figure S8) was obtained compared with beads@Ru (Figure 3B), suggesting that CNTs played a relevant role in the ECL signal enhancement. The increased intensity is demonstrated by comparing the profiles in Figure 3C, in which the turnover frequencies (TOF), *i.e.*, the normalized signals considering the different luminophore loadings between the two types of beads are also reported. TOF is the number of photons emitted in 1 s by a single luminophore, which is obtained by dividing the integrated ECL emission from the single bead by the number of luminophores present on the bead surface and by the integration time (see also supporting information and Figure S9). TOF for beads@CNT-Ru increased by 70% compared to that of beads@Ru; thus, confirming the strategical role played by CNTs in promoting enhanced ECL signals.

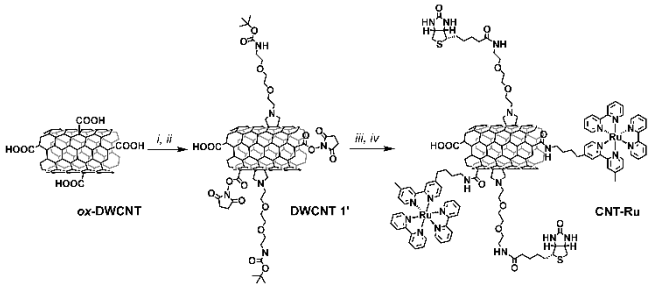

Figure 2. Schematic representation for the synthesis of f-CNTs labeled with $[Ru(bpy)_3]^{2+}$ and biotin (named CNT-Ru); *i*: paraformaldehyde, BocNH-PEG2-$NHCH_2CO_2H$, DMF, 115 °C, rt; *iia*: DIEA, EDC, DMF, rt, 1 h; *iib*: NHS, DMF, rt, 15 h; *iiia*: $Ru(bpy)_3^{2+}$ amine derivative**,** 45 °C, 24 h; *iva*: HCl:1,4-dioxane (1/2), rt; 15 h; *ivb*: EDC, NHS, biotin, MES, rt, 72 h.

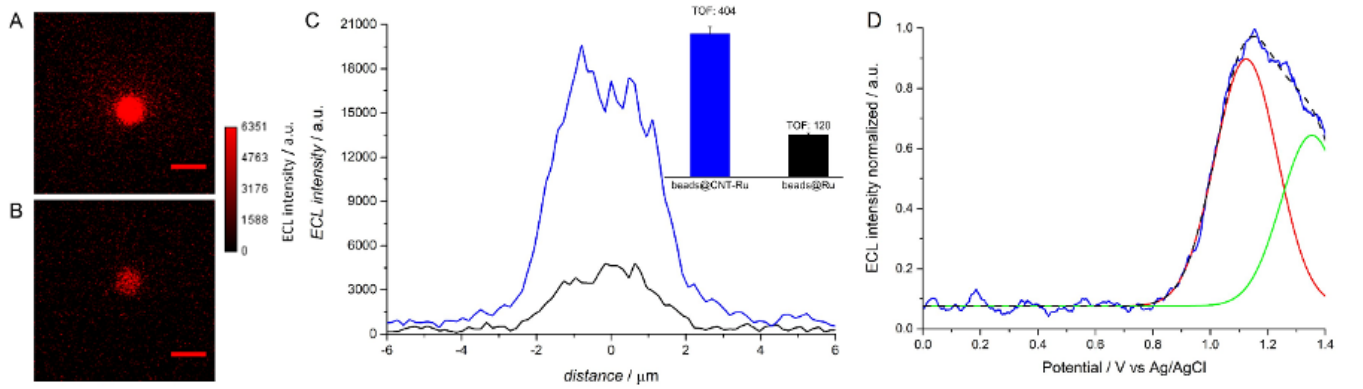

Figure 3. (A) ECL imaging of 2.8 µm single-bead labeled with CNTs labeled with $[Ru(bpy)_3]^{2+}$ (beads@CNT-Ru) and (B) with biotinylated antibody functionalized with $[Ru(bpy)_3]^{2+}$ (beads@Ru). The images were obtained by applying a constant potential of 1.4 V (vs. Ag/AgCl) for 4 s in 180 mM TPrA and 0.2 M phosphate buffer (PB). Pt wire was used as counter electrode. EMCCD camera was coupled with a potentiostat. Integration time, 8 s; magnification, X100; scale bar, 5 µm. (C) Comparison of the beads profile lines (black line, beads@Ru; blue line, beads@CNT-Ru). Inset of the comparison between TOF values calculated for beads@Ru (black) and beads@CNT-Ru (blue). Error bars show the standard error (n ≥10). (D) Cyclic voltammetry performed on beads@CNT-Ru (blue), scanning the potential between 0 V and 1.4 V and ECL emission signal acquired each 200 ms. Deconvolution of the cyclic voltammetry peak at 1 V (red line) and 1.2 V (green line), in which the TPrA and $[Ru(bpy)_3]^{2+}$ were oxidized, respectively. The sum of these two peaks deconvolution was represented by dotted black line. EMCCD camera was coupled with a potentiostat. Integration time, 200 ms.

Notice that TOF is normalized for the quantity of luminophore as it is described in detail in the supporting information. A possible explanation for the observed effect is associated with the previously observed ability of CNTs to promote the efficient anodic oxidation of amines and other substrates.[37,49–53] As shown in Figure 1A and according to the mechanism outlined above (*remote ECL, equations 1–6)*, the ECL signal depends entirely on the direct oxidation of TPrA. The CNT-Ru moieties, which are randomly distributed onto the bead surface, are likely to form a conductive electrocatalytic network, in turn electronically wired to the electrode surface, onto which TPrA oxidation may occur. This leads to an effective increase of the TPrA radicals' concentration over the whole bead surface compared with beads@Ru, in which oxidation only occurs at the electrode surface.

To confirm the above hypothesis, ECL analysis at a single-beads level was investigated substituting TPrA with dibutylaminoethanol (DBAE) as the coreactant (Figure S10). In the ECL generation mechanism, DBAE exhibited an analogous mechanism as depicted by equations 1–6. However, due to the very short lifetime of DBAE radical cation,[48] emission from beads@Ru was not observed. In contrast, in the case of beads@CNT-Ru, the presence of the CNT electrocatalytic network, at a very short distance from the luminophore, allows the sequence of processes in equations 1–6 among with the observation of a strong signal (Figure S10).

Quite unexpectedly, the analysis of the ECL signal distribution with the applied potential, as measured by acquiring the ECL signal from the individual beads (either beads@Ru or beads@CNT-Ru) during a cyclic potential scan from 0 to 1.4 V (acquisition time 200 ms), also highlighted an additional ECL generation mechanism (see the supplementary movie). Figure 3D illustrates the analysis of the case in which beads@CNT-Ru is leading an additional contribution at ~1.2-1.4 V compared with the curves related to beads@Ru (Figure S11). It may be associated with the anodic oxidation of the $[Ru(bpy)_3]^{2+}$ moieties also supported by the comparison between the electrochemical behaviour of beads@CNT-Ru and beads@Ru in absence of coreactant (see figure S12). Such an oxidation process would occur onto the CNTs surface because of the flexibility of the linker connecting the luminophore to the CNT moiety, allowing an alternative mechanism for ECL generation which is not viable with beads@Ru. Such a mechanism involves both TPrA (eq 1-3) and $[Ru(bpy)_3]^{2+}$ (eq 7-9), whose parallel oxidation leads to ECL, according to the following mechanism where the homogeneous reaction eq. 4-5 are replaced by equation 7-8.

$$TPrAH^+ \leftrightarrows TPrA + H^+ \quad (1)$$

$$TPrA - e^- \leftrightarrows TPrA^{\bullet+} \quad (2)$$

$$TPrA^{\bullet+} \leftrightarrows TPrA^{\bullet} + H^+ \quad (3)$$

$$beads@CNT\text{-}Ru^{2+} - e^- \leftrightarrows beads@CNT\text{-}Ru^{3+} \quad (7)$$

$$TPrA^{\bullet} + beads@CNT\text{-}Ru^{3+} \leftrightarrows P1 + beads@CNT\text{-}Ru^{2+*} \quad (8)$$

$$beads@CNT\text{-}Ru^{2+*} \rightarrow beads@CNT\text{-}Ru^{2+} + h\nu \quad (9)$$

This mechanism is usually observed in the homogeneous case, in which both luminophore and coreactant are free to diffuse to the electrode surface. However, this is not possible for the heterogeneous ECL, in which *remote ECL* is usually the only mechanism observed.[43] Fundamental characters in the ECL generation remain the presence of the luminophore onto the beads (Figures S13) and the application of a sufficiently high oxidation potential for overcoming the ohmic drop due to the high concentration of coreactant.[13]

Finally, the effective role played by the conductive network of CNTs in promoting enhanced ECL around the beads was further confirmed by inspecting the emission of the 4 μm diameter beads, similarly functionalized with either CNT-Ru or Ru labels (Figures S14A and B). The former displays a more homogeneous emission over the entire bead and larger ECL intensity compared with the latter (Figure S14C).

In conclusion, the insertion of CNTs (DWCNTs) as an interlayer between the luminophores and the magnetic microbead brings a significant enhancement of the ECL signal, which is a combined effect of the increased efficiency of the remote ECL mechanism, usually involved in such systems, and the concurrence of an additional ECL-generating mechanism, generally limited to homogeneous systems. A new and very promising route is opened for increasing the sensitivity of ECL immunoassays based on the ECL imaging technique.

This work was supported by the European Union's Horizon 2020 research and innovation program under Grant Agreement 881603 Graphene Flagship. This research was funded by MIUR, grant number 2017PBXPN4. Flagship. M.P., as the recipient of the AXA Bionanotechnology Chair, is grateful to the AXA Research Fund for financial support. This work was performed under the Maria de Maeztu Units of Excellence Program from the Spanish State Research Agency – Grant No. MDM-2017-0720. A.C. thanks Xunta de Galicia for his research grant Atracción de Talento (nº ED431H 2020/17).

The authors declare no competing financial interest.

1 Y. Bai, T. Shu, L. Su and X. Zhang, *Anal. Bioanal. Chem.*, 2020, **412**, 6655–6665.
2 M. Sharifi, M. R. Avadi, F. Attar, F. Dashtestani, H. Ghorchian, S. M. Rezayat, A. A. Saboury and M. Falahati, *Biosens. Bioelectron.*, 2019, **126**, 773–784.
3 L. Xu, D. Li, S. Ramadan, Y. Li and N. Klein, *Biosens. Bioelectron.*, 2020, **170**, 112673.
4 H. Qi and C. Zhang, *Anal. Chem.*, 2020, **92**, 524–534.
5 C. Ma, Y. Cao, X. Gou and J.-J. Zhu, *Anal. Chem.*, 2020, **92**, 431–454.
6 A. Juzgado, A. Soldà, A. Ostric, A. Criado, G. Valenti, S. Rapino, G. Conti, G. Fracasso, F. Paolucci and M. Prato, *J. Mater. Chem. B*, 2017, **5**, 6681–6687.
7 B. Babamiri, D. Bahari and A. Salimi, *Biosens. Bioelectron.*, 2019, **142**, 111530.
8 H. Li, L. Bouffier, S. Arbault, A. Kuhn, C. F. Hogan and N. Sojic, *Electrochem. commun.*, 2017, **77**, 10–13.
9 M. Hesari and Z. Ding, *J. Electrochem. Soc.*, 2016, **163**, H3116–H3131.
10 M. M. Richter, *Chem. Rev.*, 2004, **104**, 3003–3036.
11 W. Miao, *Chem. Rev.*, 2008, **108**, 2506–2553.
12 Roche Diagnostic corporation.
13 A. Zanut, A. Fiorani, S. Canola, T. Saito, N. Ziebart, S. Rapino, S. Rebeccani, A. Barbon, T. Irie, H.-P. Josel, F. Negri, M. Marcaccio, M. Windfuhr, K. Imai, G. Valenti and F. Paolucci, *Nat. Commun.*, 2020, **11**, 2668.
14 H. Wang, L. Liao, Y. Chai and R. Yuan, *Biosens. Bioelectron.*, 2020, **150**, 111915.
15 Y. Liu, Y. Sun and M. Yang, *Anal. Methods*, 2021, **13**, 903–909.
16 X. Wang, L. Yu, Q. Kang, L. Chen, Y. Jin, G. Zou and D. Shen, *Electrochim. Acta*, 2020, **360**, 136992.
17 C. Song, X. Li, L. Hu, T. Shi, D. Wu, H. Ma, Y. Zhang, D. Fan, Q. Wei and H. Ju, *ACS Appl. Mater. Interfaces*, 2020, **12**, 8006–8015.
18 H. Ding, W. Guo and B. Su, *Angew. Chemie*, 2020, **132**, 457–464.
19 G. Valenti, S. Scarabino, B. Goudeau, A. Lesch, M. Jović, E. Villani, M. Sentic, S. Rapino, S. Arbault, F. Paolucci and N. Sojic, *J. Am. Chem. Soc.*, 2017, **139**, 16830–16837.
20 L. C. Soulsby, D. J. Hayne, E. H. Doeven, L. Chen, C. F. Hogan, E. Kerr, J. L. Adcock and P. S. Francis, *ChemElectroChem*, 2018, **5**, 1543–1547.
21 H. Ding, W. Guo and B. Su, *Angew. Chemie Int. Ed.*, 2020, **59**, 449–456.
22 W. Zhao, H.-Y. Chen and J.-J. Xu, *Chem. Sci.*, , DOI:10.1039/D0SC07085H.
23 H. Ding, P. Zhou, W. Fu, L. Ding, W. Guo and B. Su, *Angew. Chemie Int. Ed.*, 2021, anie.202101467.
24 L. Xu, Y. Li, S. Wu, X. Liu and B. Su, *Angew. Chemie - Int. Ed.*, 2012, **51**, 8068–8072.
25 K. Kadimisetty, I. M. Mosa, S. Malla, J. E. Satterwhite-Warden, T. M. Kuhns, R. C. Faria, N. H. Lee and J. F. Rusling, *Biosens. Bioelectron.*, 2016, **77**, 188–193.
26 S. Voci, B. Goudeau, G. Valenti, A. Lesch, M. Jović, S. Rapino, F. Paolucci, S. Arbault and N. Sojic, *J. Am. Chem. Soc.*, 2018, **140**, 14753–14760.
27 F.-R. F. Fan and A. J. Bard, *Nano Lett.*, 2008, **8**, 1746–1749.
28 Z. Chen and Y. Zu, *J. Phys. Chem. C*, 2008, **112**, 16663–16667.
29 Z. Guo, Y. Sha, Y. Hu, Z. Yu, Y. Tao, Y. Wu, M. Zeng, S. Wang, X. Li, J. Zhou and X. Su, *Anal. Bioanal. Chem.*, 2016, **408**, 7203–7211.
30 J. Lu, L. Wu, Y. Hu, S. Wang and Z. Guo, *J. Electrochem. Soc.*, 2017, **164**, B421–B426.
31 C. Ma, M.-X. Wang, H.-F. Wei, S. Wu, J.-R. Zhang, J.-J. Zhu and Z. Chen, *Chem. Commun.*, 2021, **57**, 2168–2171.
32 A. Zanut, A. Fiorani, S. Rebeccani, S. Kesarkar and G. Valenti, *Anal. Bioanal. Chem.*, , DOI:10.1007/s00216-019-01761-x.
33 A. Fiorani, D. Han, D. Jiang, D. Fang, F. Paolucci, N. Sojic and G. Valenti, *Chem. Sci.*, 2020, **11**, 10496–10500.
34 W. Guo, P. Zhou, L. Sun, H. Ding and B. Su, *Angew. Chemie Int. Ed.*, 2021, **60**, 2089–2093.
35 H. Ju, N. Wang, H. Gao, Y. Li, G. Li, W. Chen, Z. Jin, J. Lei and Q. Wei, *Angew. Chemie Int. Ed.*, , DOI:10.1002/anie.202011176.
36 Z. Guo, Y. Sha, Y. Hu and S. Wang, *Chem. Commun.*, 2016, **52**, 4621–4624.
37 A. Fiorani, J. P. Merino, A. Zanut, A. Criado, G. Valenti, M. Prato and F. Paolucci, *Curr. Opin. Electrochem.*, 2019, **16**, 66–74.
38 A. Zanut, F. Palomba, M. Rossi Scota, S. Rebeccani, M. Marcaccio, D. Genovese, E. Rampazzo, G. Valenti, F. Paolucci and L. Prodi, *Angew. Chemie Int. Ed.*, 2020, **59**, 21858–21863.
39 G. Valenti, A. Fiorani, H. Li, N. Sojic and F. Paolucci, *ChemElectroChem*, 2016, **3**, 1990–1997.
40 G. Valenti, E. Rampazzo, S. Kesarkar, D. Genovese, A. Fiorani, A. Zanut, F. Palomba, M. Marcaccio, F. Paolucci and L. Prodi, *Coord. Chem. Rev.*, 2018, **367**, 65–81.
41 S. Voci, H. Al-Kutubi, L. Rassaei, K. Mathwig and N. Sojic, *Anal. Bioanal. Chem.*, 2020, **412**, 4067–4075.
42 S. Zhang, R. Geryak, J. Geldmeier, S. Kim and V. V. Tsukruk, *Chem. Rev.*, 2017, **117**, 12942–13038.
43 W. Miao, J.-P. Choi and A. J. Bard, *J. Am. Chem. Soc.*, 2002, **124**, 14478–14485.
44 P. Dutta, D. Han, B. Goudeau, D. Jiang, D. Fang and N. Sojic, *Biosens. Bioelectron.*, 2020, **165**, 112372.
45 J. K. Leland and M. J. Powell, *J. Electrochem. Soc.*, 1990, **137**, 3127–3131.
46 Y. Zu and A. J. Bard, *Anal. Chem.*, 2000, **72**, 3223–3232.
47 L. S. Dolci, S. Zanarini, L. Della Ciana, F. Paolucci and A. Roda, *Anal. Chem.*, 2009, **81**, 6234–6241.
48 M. Sentic, M. Milutinovic, F. Kanoufi, D. Manojlovic, S. Arbault and N. Sojic, *Chem. Sci.*, 2014, **5**, 2568–2572.
49 G. Valenti, M. Zangheri, S. E. Sansaloni, M. Mirasoli, A. Penicaud, A. Roda and F. Paolucci, *Chem. - A Eur. J.*, 2015, **21**, 12640–12645.
50 V. A. Zamolo, G. Valenti, E. Venturelli, O. Chaloin, M. Marcaccio, S. Boscolo, V. Castagnola, S. Sosa, F. Berti, G. Fontanive, M. Poli, A. Tubaro, A. Bianco, F. Paolucci and M. Prato, *ACS Nano*, 2012, **6**, 7989–7997.
51 R. Wang, H. Wu, R. Chen and Y. Chi, *Small*, 2019, **15**, 1901550.
52 L. Yang, A. D. Hendsbee, Q. Xue, S. He, C. R. De-Jager, G. Xie, G. C. Welch and Z. Ding, *ACS Appl. Mater. Interfaces*, 2020, **12**, 51736–51743.
53 K. Kadimisetty, S. Malla, K. S. Bhalerao, I. M. Mosa, S. Bhakta, N. H. Lee and J. F. Rusling, *Anal. Chem.*, 2018, **90**, 7569–7577.